Influence of Zn$_{1-x}$Ca$_x$WO$_4$ heterostructures synthesized by spray pyrolysis on photoluminescence property

A.A.G. Santiago[a,*], Y.L.R.L. Fernandes[a], R.L. Tranquilin[a], E. Longo[b], C.A. Paskocimas[a], F.V. Motta[a], M.R.D. Bomio[a]

[a] LSQM – Laboratory of Chemical Synthesis of Materials, Department of Materials Engineering, Federal University of Rio Grande Do Norte, UFRN, P.O. Box 1524, Natal, RN, Brazil
[b] CDMF-UFSCar, Universidade Federal de São Carlos, P.O. Box 676, 13565-905, São Carlos, SP, Brazil

A B S T R A C T

Tungstates are inorganic materials with great potential in diverse applications, mainly as a photoluminescent material as a candidate to replace traditional lighting sources. In this study, we report the synthesis and characterization of Zn$_{1-x}$Ca$_x$WO$_4$ (x = 0, 0.2, 0.4, 0.6, 0.8, and 1) powders with white light-emitting properties. Using X-ray diffraction, the formation of the monoclinic ZnWO$_4$ phase was observed for x = 0 and the formation of the tetragonal scheelite phase of CaWO$_4$ was observed for x = 1. The formation of a heterostructure composed of both phases was found for compositions with x = 0.2, 0.4, 0.6 and 0.8. Scanning electron microscopy images showed that the Zn$_{1-x}$Ca$_x$WO$_4$ particles exhibit a spherical morphology. The band-gap energies had variation between 3.79 eV and 3.99 eV, being influenced by the degree of structural disorder. The photoluminescence emission spectra of the samples showed white light emission. Thus, Zn$_{1-x}$Ca$_x$WO$_4$ can be considered as promising white light sources, mainly for the sample synthesized with x = 0.8 for application in LED lamps (6500 K).

1. Introduction

The area of research and development of new materials has been extremely competitive and constantly updated in recent years, and in this scenario the study of semiconductors with photoluminescent properties has also intensified, mainly to improve the efficiency of the components for applications in the LED industry, lasers and for screens of electronic devices, for example [1–4]. Thus, metallic tungstates have been used in diverse potential applications such as optical fibers, humidity sensors, photoluminescence, lasers, and X-Ray intensifying screens [5–7]. Tungstates can have two types of structures: monoclinic, in which the tungsten atoms and the metal ions are coordinated by six oxygen atoms forming octahedra groups of [WO$_6$] and [AO$_6$]; and tetragonal, in which the tungsten atoms are coordinated by four oxygen atoms forming tetrahedra [WO$_4$], whereas the metal ions have eight oxygen atoms, forming deltahedron [AO$_8$] [8,9].

Zinc tungstate (ZnWO$_4$) is a promising metallic tungstate which has a monoclinic structure and exhibits intrinsic emission of blue-green coloration when excited by UV radiation [10–12]. However, calcium tungstate (CaWO$_4$) is an important tungstate and has a tetragonal Scheelite structure. CaWO$_4$ exhibits excellent optical properties with efficient blue, violet or green light emission when excited by ultraviolet

radiation to x-rays [13–15].

These tungstates have good chemical stability and high photosensitivity and are therefore used in screens for electronic devices, nanocomposites, lasers, devices for medical treatments, magnetic nanomaterials, sensors, field emission devices, optical fibers, LEDs and scintillation detectors. These different applications occur because tungstates are highly influenced by the synthesis method, time and temperature used to obtain them, resulting in variations in the structural network, morphology, size, and porosity of the particles [16–20].

Consequently, several synthesis methods have been used to obtain tungstates such as co-precipitation, conventional and microwave-assisted hydrothermal, solvothermal, solid-state reaction, sol-gel, combustion and spray pyrolysis [21–27]. The ultrasonic spray pyrolysis (USP) method is a simple, fast and continuous method consisting of three basic steps: the atomization of the precursor solution, heat treatment, and collection of the precipitates [28,29]. This method has the main advantages of producing materials with high purity, high homogeneity, spherical morphology, a short processing period and easy control of the average particle size [30–32]. Therefore, the ultrasonic spray pyrolysis method is an excellent alternative to obtaining in one-step heterostructured materials.

In this study we report obtaining Zn$_{1-x}$Ca$_x$WO$_4$ (x = 0, 0.2, 0.4, 0.6,

* Corresponding author.
  E-mail address: andersonsantiago@ufrn.edu.br (A.A.G. Santiago).

0.8, and 1) powder prepared by the USP method. These powders present a heterostructure formed by the $ZnWO_4$ and $CaWO_4$ phases, resulting in a material which has the photoluminescent properties of both phases. The characterization of its structural, morphological and optical properties at room conditions was realized by means of x-ray diffraction (XRD), field-emission scanning electron microscopy (FE-SEM), photoluminescence (PL) and UV–Vis reflectance measurements.

2. Experimental details

2.1. Materials

Zinc nitrate hexahydrate $[Zn(NO_3)_2 \cdot 6H_2O]$ (Sigma-Aldrich, 98% purity), calcium nitrate tetrahydrate $[Ca(NO_3)_2 \cdot 4H_2O]$ (Synth, 99% purity), tungstic acid $[H_2WO_4]$ (Aldrich Chemistry, 99% purity), ammonium hydroxide $[NH_4OH, 30\%]$ (Synth), nitric acid $[HNO_3, 65\%]$ (Synth), and distilled water were used as reagents to synthesize $Zn_{1-x}Ca_xWO_4$.

2.2. The synthesis procedure of $Zn_{1-x}Ca_xWO_4$ powders

Powder samples of $Zn_{1-x}Ca_xWO_4$ ($x = 0$, 0.2, 0.4, 0.6, 0.8, and 1), hereafter noted as ZWO, ZC2WO, ZC4WO, ZC6WO, ZC8WO, and CWO, respectively, were prepared by using the USP method. First, solution A was prepared by adding 5 mmol of H_2WO_4 in 25 ml of H_2O and mixed by a magnetic stirrer at 25 °C, then the pH was adjusted to 12 with NH_4OH obtaining a white and translucent solution. Next, HNO_3 was added in solution A to adjust the pH to 5. Solution B was prepared by adding 5 $(1-x)$ mmol of $Zn(NO_3)_2$ and $5(x)$ mmol of $Ca(NO_3)_2$ in 175 ml of H_2O and mixed by a magnetic stirrer at 25 °C, maintaining the pH at 5. Then, solution A was added dropwise into solution B to obtain the precursor solution. Lastly, the precursor solution was atomized using an ultrasonic nebulizer (frequency of 2.4 MHz) and airflow (3 L min^{-1}), and heating temperatures from 600 °C for zone 1 and 800 °C for zone 2. More details on the equipment and technique used are in references [33–35].

2.3. Characterization of $Zn_{1-x}Ca_xWO_4$ powders

Powder XRD patterns of $Zn_{1-x}Ca_xWO_4$ were collected within the 10° to 120° angular range with step speed of 0.02° min^{-1} using an XRD 7000 Shimadzu diffractometer and monochromatic Cu Kα ($\lambda = 1.5406$ Å) radiation. The diffraction patterns were analyzed by the General Structure Analysis System (GSAS) with an EXPGUI graphic interface [36] in order to perform the Rietveld refinement [37] and analyze the possible structural modifications. The following parameters were refined: scaling factor and phase fraction; background (displaced Chebyshev polynomial function); peak shape (Thomson-Cox-Hasting pseudo-Voigt); change in the network constants; fractional atomic coordinates; and isotropic thermal parameters. The powder morphology was examined using an FE-SEM (Carl Zeiss, model Supra 35-VP) operating at 6 kV. The UV–Vis reflectance spectrum was obtained using a UV–Vis spectrometer (Shimadzu, model UV-2600) and PL spectra were measured using a Thermal Jarrell-Ash Monospec 27 monochromator and a Hamamatsu R446 photomultiplier. The excitation source used was a krypton laser with a wavelength of 325 nm (Coherent Innova) and an output of approximately 13.3 mW.

3. Results and discussion

3.1. Structural characterization

The XRD patterns of $Zn_{1-x}Ca_xWO_4$ ($x = 0$, 0.2, 0.4, 0.6, 0.8, and 1) samples are shown in Fig. 1. The ZWO sample was indexed in a unit cell with a monoclinic wolframite-type structure with space group $P12/c1$ (number 13) in agreement with JCPDS 15–774 and the literature
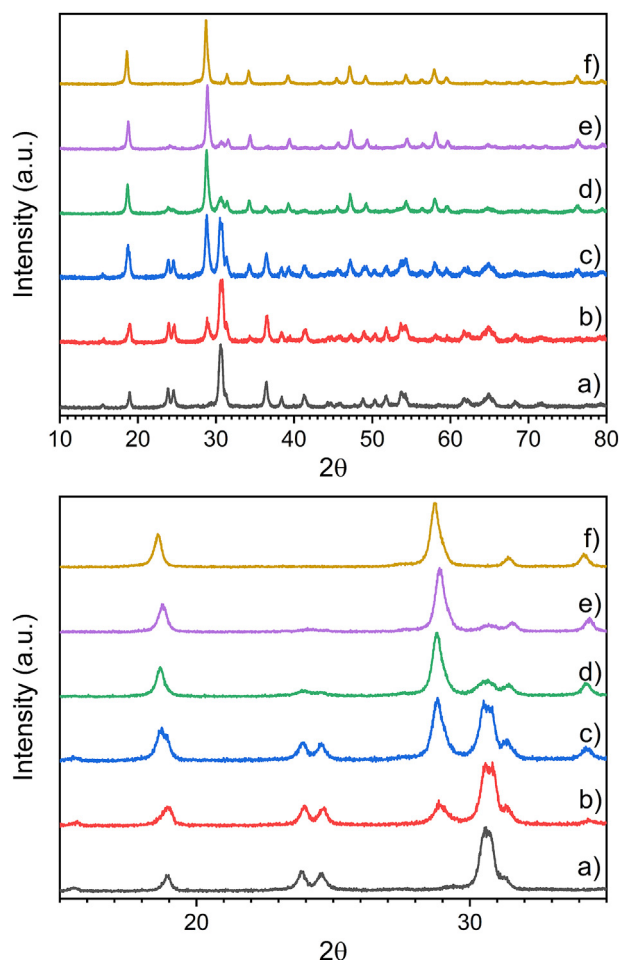

Fig. 1. XRD patterns of $Zn_{1-x}Ca_xWO_4$ being (a) ZWO, (b) ZC2WO, (c) ZC4WO, (d) ZC6WO, (e) ZC8WO and (f) CWO.

[38,39]. However, the CWO sample was indexed in a unit cell with a tetragonal scheelite-type structure with space group $P41/a$ (number 88) in agreement with JCPDS 41–1431 and the literature [40,41]. On the other hand, the ZC2WO, ZC4WO, ZC6WO, and ZC8WO samples present the coexistence of both structures, forming a heterostructure, with all Bragg peaks being indexed either with the monoclinic or the tetragonal structures. Note that the fraction of the monoclinic phase decreases with increasing the value of x since there is an increase in the substitution of Zn^{2+} cations by Ca^{2+} cations in the heterostructure.

Fig. 2 and Table 1 show the results obtained from the Rietveld refinement of XRD patterns of the different samples. The XRD pattern of the ZWO sample was well matched to ICSD 84540 ($ZnWO_4$ with monoclinic structure). The diffraction pattern for the CWO sample was well matched to ICSD 18135 ($CaWO_4$ with tetragonal structure), while the ZC2WO, ZC4WO, ZC6WO, and ZC8WO samples were well matched to a combination of both ICSD 84540 and ICSD 18135, hence forming a heterostructure.

Small variations in the structural parameters were observed between samples as the unit-cell parameter, crystallite size, and displacement of the atomic positions within the crystalline structure. These phenomena may be associated with defects produced during the USP process such as generating oxygen vacancies, possible substitutions of Ca^{2+} ions for Zn^{2+} ions in the tetragonal structure and vice versa, distortions in the $[WO_6]^{2-}$ and/or $[WO_4]^{2-}$ clusters, and the interface itself between the two phases of the heterostructure. Fig. 3 shows a representation of the unit cells of the different $Zn_{1-x}Ca_xWO_4$ powder samples and in particular the distortions in the $[WO_6]^{2-}$ and/or $[WO_4]^{2-}$ clusters for the different values of x.
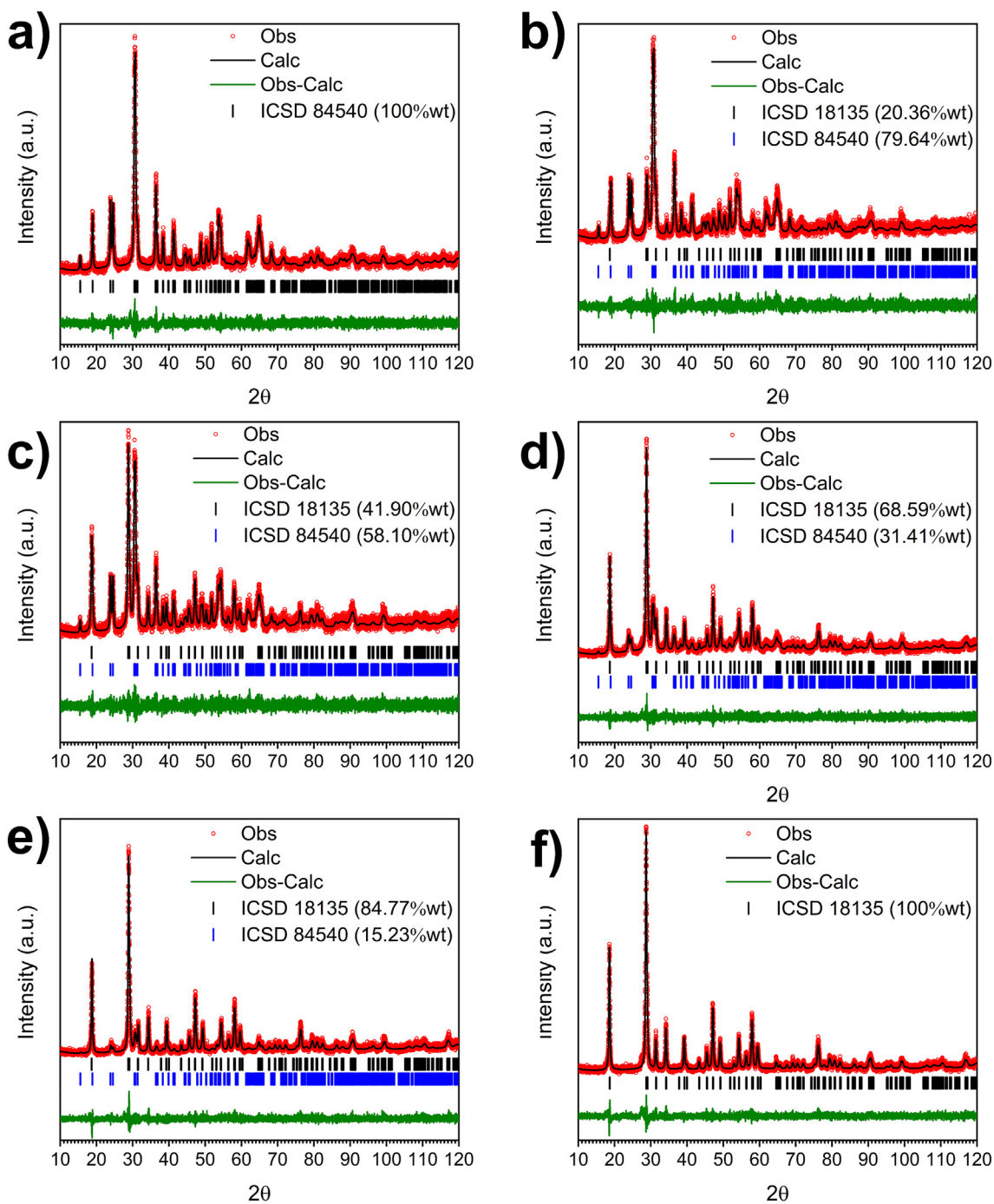
Fig. 2. Refinement graphs of $Zn_{1-x}Ca_xWO_4$ being (a) ZWO, (b) ZC2WO, (c) ZC4WO, (d) ZC6WO, (e) ZC8WO and (f) CWO.

3.2. Morphological characterization

Fig. 4 shows the micrographs of the $Zn_{1-x}Ca_xWO_4$ powder samples. The morphology of $Zn_{1-x}Ca_xWO_4$ powders is mainly composed of microspheres-shape particles. Moreover, slight holes and pores are observed on the surface of the particles. The microspheres of ZWO (Fig. 4a) exhibit a slightly porous surface, while the microspheres of CWO (Fig. 4f) exhibit a slightly smooth surface. The ZC2WO, ZC4WO, ZC6WO and ZC8WO microspheres (Fig. 4b–e) consequently show variations in morphology between ZWO and CWO.

During the USP process, the droplets experience different physicochemical phenomena such as evaporation and diffusion of solvent on the surface of the droplet, and metal nitrates melting. In addition, the metal nitrates tend to melt before the solvent evaporates completely, trapping the solvent in a droplet of molten salt, generating hollow and/or porous particles. Also, metal nitrates tend to form a high number of nanocrystallites in forming the microspheres due to the high degree of supersaturation [42].

The precursor reagents used were zinc nitrate and calcium nitrate, which present high solubility in water (1.20 g/ml of H_2O and 1.44 g/ml H_2O, respectively [43]), and this favors nanocrystals forming which compose observed the microsphere. Thus, the $Zn_{1-x}Ca_xWO_4$ microspheres are hollow and porous, formed by nanocrystals from the metal nitrates of the precursor solution.

Table 1
Refined Rietveld structural parameters for the $Zn_{1-x}Ca_xWO_4$.

Compounds	ZWO	ZC2WO	ZC2WO	ZC4WO	ZC4WO
Crystal system	Monoclinic	Monoclinic	Tetragonal	Monoclinic	Tetragonal
Space Group	*P12/c1*	*P12/c1*	*I41/a*	*P12/c1*	*I41/a*
Lattice parameters (Å)					
a	4.693	4.702	5.238	4.700	5.240
b	5.723	5.726	5.238	5.722	5.240
c	4.930	4.931	11.39	4.929	11.39
c/a			2.174		2.174
α	90.00	90.00	90.00	90.00	90.00
β	90.65	90.75	90.00	90.74	90.00
γ	90.00	90.00	90.00	90.00	90.00
$V(Å^3)$	132.4	132.8	312	132.5	312.7
χ^2	1.199	1.247	1.247	1.181	1.181
Rp (%)	9.27	10.43	10.43	9.13	9.13
RF^2 (%)	10.17	17.48	17.48	14.77	14.77
D (nm)	20.4	20.4	15.1	18.2	16.0
ε $(x10^{-3})$	1.18	1.19	1.54	1.30	1.47

Compounds	ZC6WO	ZC6WO	ZC8WO	ZC8WO	CWO
Crystal syste m	Monoclinic	Tetragonal	Monoclinic	Tetragonal	Tetragonal
Space Group	*P12/c1*	*I41/a*	*P12/c1*	*I41/a*	*I41/a*
Lattice parameters (Å)					
a	4.703	5.239	4.704	5.239	5.241
b	5.721	5.239	5.710	5.239	5.241
c	4.931	11.39	4.928	11.38	11.38
c/a		2.174		2.172	2.171
α	90.00	90.00	90.00	90.00	90.00
β	90.74	90.00	90.46	90.00	90.00
γ	90.00	90.00	90.00	90.00	90.00
$V(Å^3)$	132.7	312.6	132.4	312.5	312.6
χ^2	1.220	1.220	1.262	1.262	1.244
Rp (%)	9.16	9.16	10.76	10.76	9.25
RF^2 (%)	13.95	13.95	16.82	16.82	10.36
D (nm)	11.3	18.0	9.33	19.6	19.4
ε $(x10^{-3})$	2.13	1.31	2.64	1.20	1.22

3.3. Optical characterization

3.3.1. UV–visible spectroscopy

Fig. 5 shows the estimated values for the band gap energy of Zn_{1-} $_xCa_xWO_4$ samples. The gap energy values (E_{gap}) were estimated using the Kubelka-Munk function [44] followed by the Wood and Tauc method [45]. The optical band gap energy is assumed by $\alpha h\nu \propto (h\nu - E_{gap})^{1/k}$ [45], where α is the absorbance, h is the Planck constant, ν is
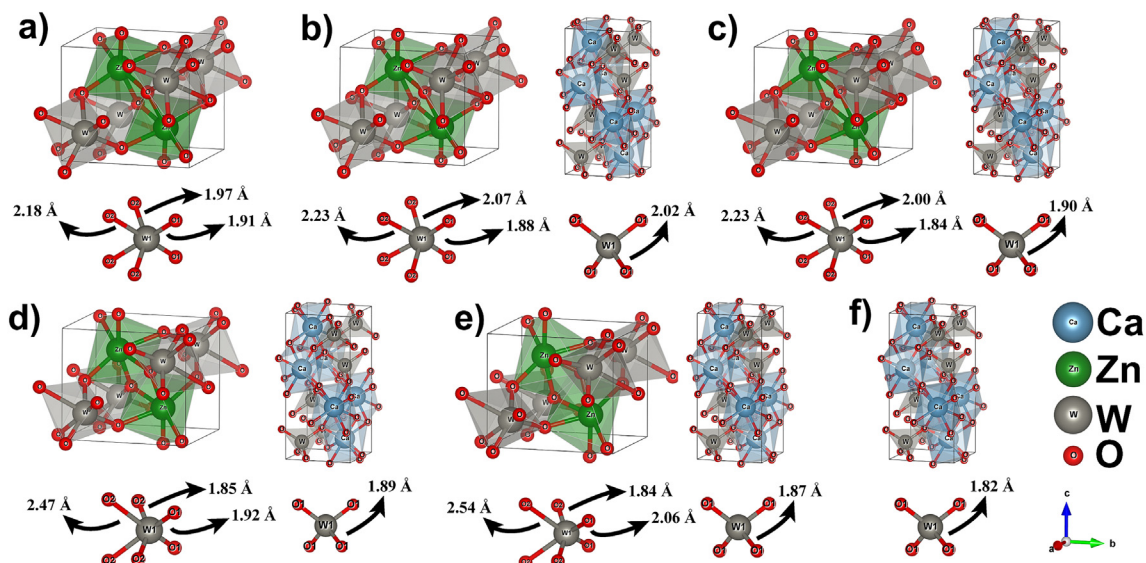
Fig. 3. Structural modeling of the $Zn_{1-x}Ca_xWO_4$ being (a) ZWO, monoclinic structure; (b) ZC2WO, monoclinic and tetragonal structures; (c) ZC4WO, monoclinic and tetragonal structures; (d) ZC6WO, monoclinic and tetragonal structures; (e) ZC8WO, monoclinic and tetragonal structures; and (f) CWO, tetragonal structure.
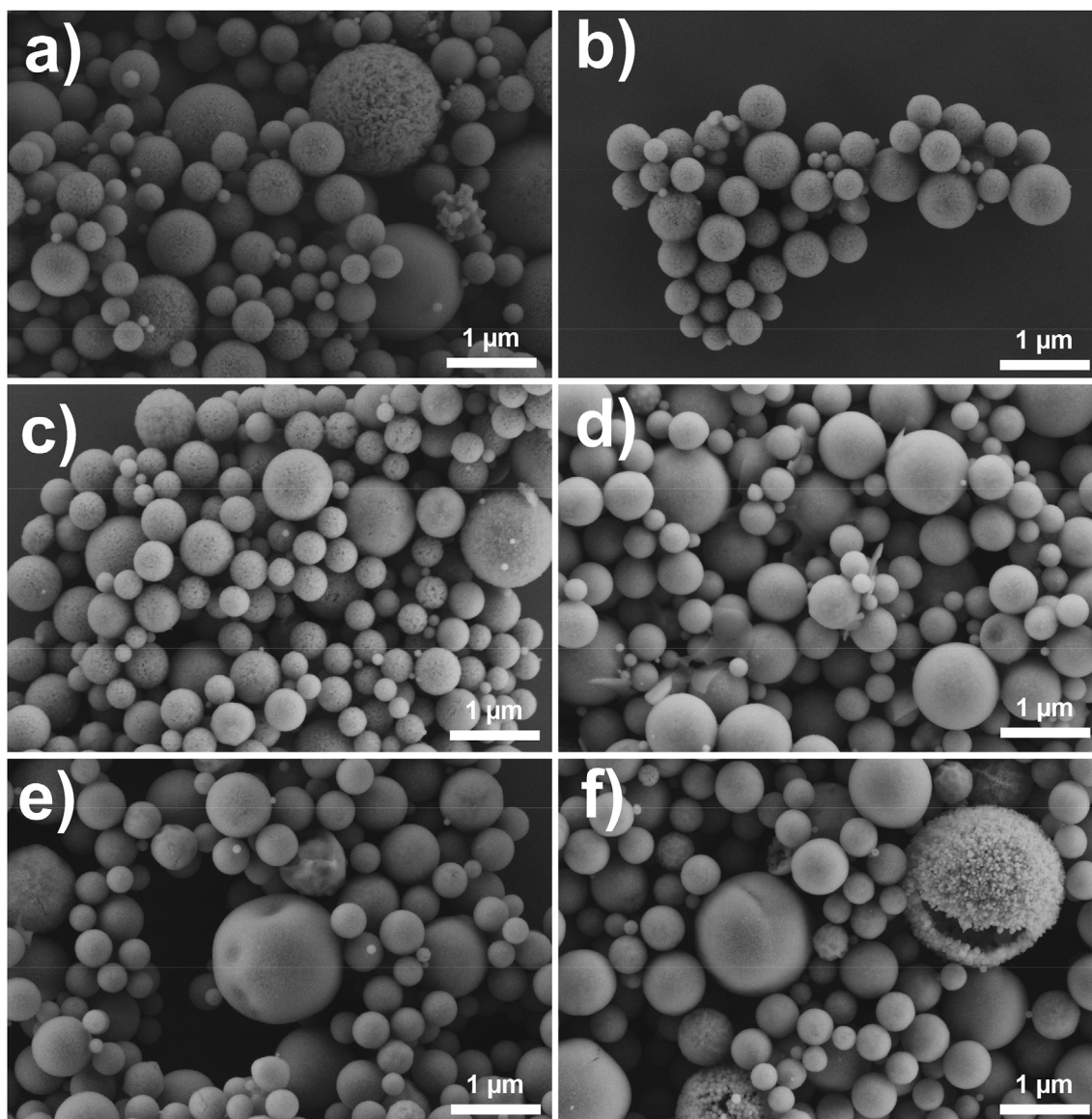
Fig. 4. FE-SEM micrographs of $Zn_{1-x}Ca_xWO_4$ powders being (a) ZWO, (b) ZC2WO, (c) ZC4WO, (d) ZC6WO, (e) ZC8WO, and (f) CWO.

the frequency, and k is indicated for the different kind of transitions. Tungstates are typically reported with permitted direct electronic transition [46–49], so the results from $Zn_{1-x}Ca_xWO_4$ samples were analyzed assuming $k = 1/2$, which is the expected value for such transitions.

The estimated values for samples are according to the literature. Experimentally, Xiong et al. [50] and Sethi et al. [51] synthesized $ZnWO_4$ and obtained band gap values of 4.93 eV (solid-state method) and 3.48 eV (hydrothermal method), respectively. On the other hand, Manjunath and Thimmanna [52], and Sahmi et al. [53] synthesized $CaWO_4$ and obtained band gap values of 3.59 eV (combustion method) and 4.88 eV (nitrate route), respectively. Han et al. [18] and Ben-makhlouf et al. [54] calculated theoretically the bandgap these tungstates utilizing the density-functional theory (DFT) and obtained values of ~4.019 eV to $ZnWO_4$ and 4.03 eV to $CaWO_4$, respectively.

The band-gap of tungstates (AWO_4) is generally dominated by $W^{6+}(5d)$ states in conduction bands and $O^{2-}(2p)$ states in valence bands [55]. These states are strongly influenced by the degree of structural order-disorder, as tungstates present a low number of inter-mediate levels between the conduction band and valence band [56]. Thus, the greater the structural disorder, the lower the tungstate band

gap will be due to the increase of intermediate levels. In addition, the ionic radius of the A^{2+} metal is proportional to the tungstate band-gap, because the hybridization state of the electrons is affected [57].

The ZWO sample (Fig. 6a) shows 3.88 eV, while CWO (Fig. 6f) presents 3.99 eV. However, the ZC2WO, ZC4WO, ZC6WO, and ZC8WO samples have intermediate band gaps due to the proportion and inter-face between heterostructure phases and the defects generated during the process such as oxygen vacancies and distortions in $[WO_6]^{2-}/[WO_4]^{2-}$ clusters.

3.3.2. Photoluminescence (PL)

PL emission spectra were realized with excitation of 325 nm at ambient temperature and Fig. 6 shows the spectra obtained from the $Zn_{1-x}Ca_xWO_4$ samples. All samples exhibit a broadband PL spectrum. This emission profile is defined as the multiphonon and multilevel process, in which the relaxation involved in the participation of several energy states within the band gap of the material occurs [58]. More-over, the PL intensity decreased with the increase of Ca^{2+} cations; Almeida et al. [59] observed similar behavior, where the doping of Zn^{2+} in $CaWO_4$ increased PL emission and decreased unit cell volume.

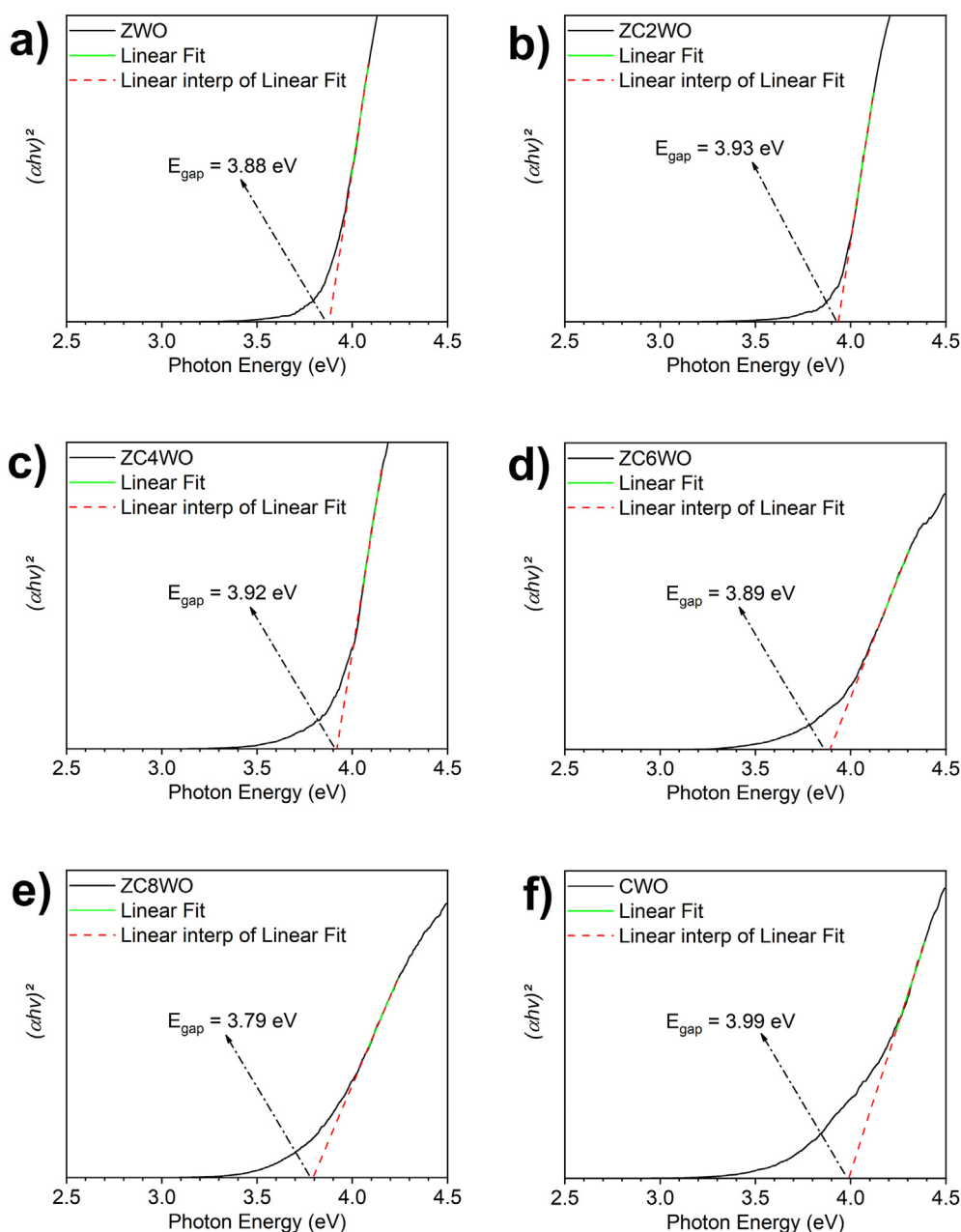The PL emission of tungstates with monoclinic wolframite-type

Fig. 5. UV–Vis absorbance spectra of $Zn_{1-x}Ca_xWO_4$ powders being (a) ZWO, (b) ZC2WO, (c) ZC4WO, (d) ZC6WO, (e) ZC8WO, and (f) CWO.

structure occurs because of the charge transfer in the [WO$_6$] clusters, while this charge transfer occurs in the [WO$_4$] clusters for tungstates with a tetragonal scheelite-type structure, in which the energy is absorbed from O 2p orbitals and is promoted from W 5d orbitals to both structures [60,61]. According to the literature, the yellow-red emission is associated with deep defects, structural disorder and oxygen vacancies in [WO$_6$]/[WO$_4$] clusters, while the blue-green emission is associated with shallow defects, intrinsic emission and structural ordering [10,62–64]. Thus, the deconvolution of the Gaussian curves of the $Zn_{1-x}Ca_xWO_4$ samples was performed using PeakFit 4.12 software with the intention to estimate the contribution of each color in the PL spectra, as can be seen in Fig. 7.

The deconvolutions propose that ZWO, ZC2WO, ZC4WO, ZC6WO, and ZC8WO samples have a predominance of PL emission in the green region while the CWO sample has a predominance in the blue region. It is also possible to observe that ZC2WO, ZC4WO, ZC6WO, and ZC8WO samples have intermediary PL spectra between ZWO and CWO. This

occurs due to the proportion of each phase within the heterostructure, as well as defects generated during the charge formation and transfer at the interface between the phases. Thus, the blue-green emission is associated with shallow defects and structural ordering while the orange-red emission is associated with deep defects, structural disorder and oxygen vacancies in [$WO_5 \cdot V_o^x$] and/or [$WO_3 \cdot V_o^x$] clusters.

The CIE chromatic (x, y) coordinates were used to verify the color emitted by the spectrum of samples. Fig. 8 shows the results of CIE (x, y) coordinate of $Zn_{1-x}Ca_xWO_4$ powders while Table 2 presents the CIE coordinates values, correlation color temperature (CCT) and the color emitted from each sample.

Materials to be applied in white LEDs have to present CCT values between 4000 and 8000 K for the color emission to be neutral- and cool-white. Only the ZC4WO sample went outside the white light emission range. Obtaining phosphorus with white emission has mainly been explored utilizing rare earth (RE) elements as dopants of the tungstate matrix. Zhai et al. [65] obtained ZnWO$_4$:(0.02 mol Eu, 0.025 mol Dy)
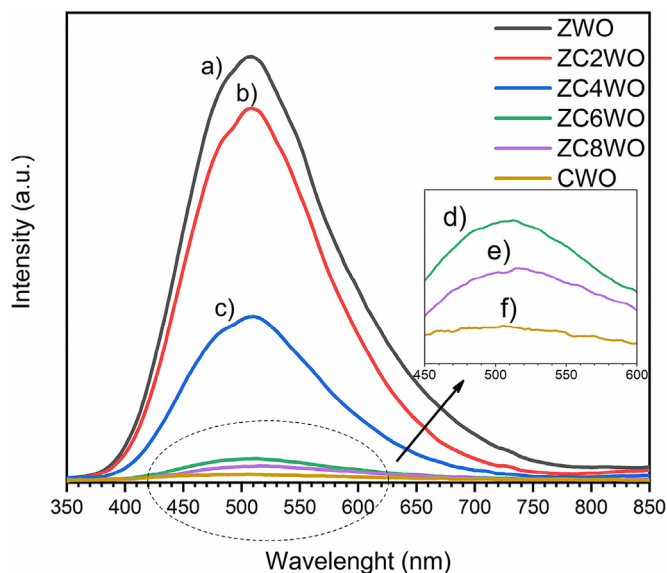
Fig. 6. PL spectra of $Zn_{1-x}Ca_xWO_4$ powders being (a) ZWO, (b) ZC2WO, (c) ZC4WO, (d) ZC6WO, (e) ZC8WO, and (f) CWO.

by the hydrothermal method, obtaining a CCT response of 6310 K. Yaba et al. [66] also utilized the hydrothermal method in synthesizing $CaWO_4$:(0.07 mol Dy) with CIE coordinates of x = 0.32 and y = 0.34. Barbosa et al. [67] synthesized $CaWO_4$:(0.02 mol Tb, 0.02 mol Eu, 0.02 mol Dy) by the coprecipitation method, obtaining a CCT response of 5933 K. The RE use has been questioned due to their expressive toxicity and prolonged exposure which can induce pulmonary complications such as bronchiolar, alveolar and interstitial histological reactions [68,69]. Thus, obtaining materials with white emission and without RE is required for biological reasons. Therefore, the $Zn_{1-x}Ca_xWO_4$ heterostructure can be presented as an alternative for
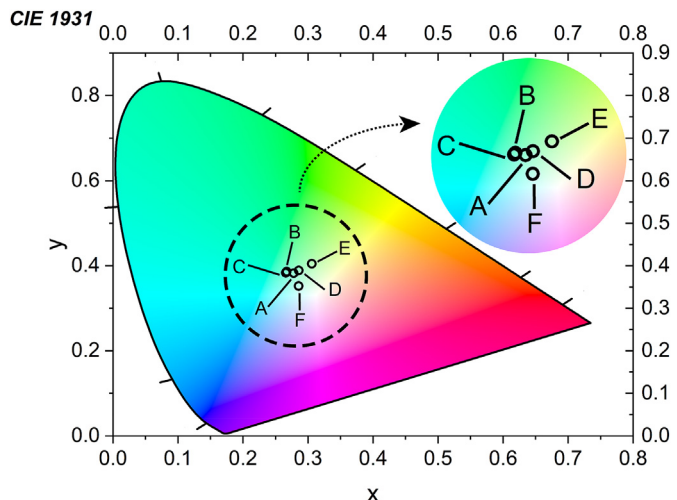

Fig. 8. CIE of $Zn_{1-x}Ca_xWO_4$ powders being (A) ZWO, (B) ZC2WO, (C) ZC4WO, (D) ZC6WO, (E) ZC8WO, and (F) CWO.

Table 2
Coordinates of CIE, CCT and color emission of $Zn_{1-x}Ca_xWO_4$.

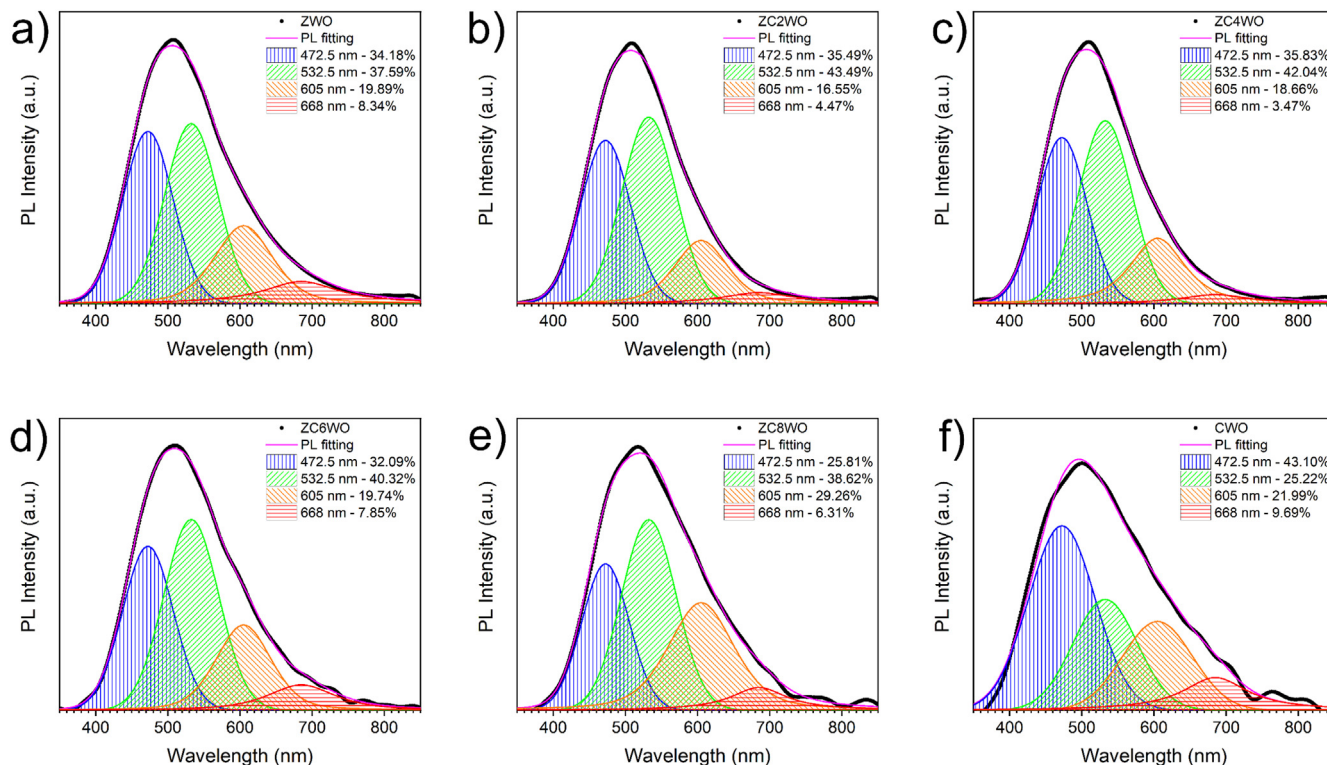| Sample	x	y	CCT (K)	Color
ZWO	0.28	0.38	7634	Average summer shade
ZC2WO	0.27	0.39	7982	Average summer shade
ZC4WO	0.27	0.38	8087	Average summer shade
ZC6WO	0.29	0.39	7231	Light summer shade
ZC8WO	0.31	0.40	6373	Summer sunlight (and blue sky, Xenon-lamp)
CWO	0.29	0.35	7689	Average summer shade

Fig. 7. Deconvolution of PL curves of $Zn_{1-x}Ca_xWO_4$ powders being (a) ZWO, (b) ZC2WO, (c) ZC4WO, (d) ZC6WO, (e) ZC8WO, and (f) CWO.

phosphorus without RE, mainly the ZC8WO sample because its CCT value is close to that of LED commercial lamps (6500 K).

4. Conclusion

The $Zn_{1-x}Ca_xWO_4$ (x = 0, 0.2, 0.4, 0.6, 0.8, and 1) samples were successfully obtained by the ultrasonic spray pyrolysis method. XRD patterns showed that the sample with ZWO has a monoclinic structure ($ZnWO_4$) and the sample with CWO has a scheelite tetragonal structure ($CaWO_4$), while the samples with x = 0.2 to 0.8 showed the formation of a monoclinic/tetragonal heterostructure. The $Zn_{1-x}Ca_xWO_4$ particles presented spherical morphology with x = 0 exhibiting a slightly porous surface, while x = 1 exhibited a slightly smooth surface. The band-gap of the ZWO (CWO) sample was 3.88 eV (3.99 eV), while samples with x = 0.2 to 0.8 showed intermediate values which seem to be highly influenced by the degree of structural disorder. The PL emission spectra of the samples showed predominance in the green-blue emission but only the ZC4WO sample did not emit in the white range of CCT (4000–8000 K). The $Zn_{1-x}Ca_xWO_4$ samples can be considered promising white light sources, mainly the ZC8WO sample which presented emission near 6500 K.

Acknowledgment

References

[1] R.F. Gonçalves, L.S. Cavalcante, I.C. Nogueira, E. Longo, M.J. Godinho, J.C. Sczancoski, V.R. Mastelaro, I.M. Pinatti, I.L.V. Rosa, A.P.A. Marques, Rietveld refinement, cluster modelling, growth mechanism and photoluminescence properties of CaWO4:Eu3+ microcrystals, CrystEngComm 17 (2015) 1654–1666.

[2] M. Murayama, K. Yoda, K. Shiraishi, I.F. Crowe, S. Komuro, X. Zhao, Photoluminescence enhancement and change in the second nearest neighbor distance of Sm-doped TiO2 thin films, Phys. Status Solidi 256 (2019) 1800522.

[3] F.B. Xiong, L.X. Lin, H.F. Lin, X.G. Meng, S.Y. Lian, W.Z. Zhu, Synthesis and photoluminescence of Mn4+ in M4Al14O25 (M = Sr or Mg) compounds as red-light phosphors for white LED, Opt. Laser. Technol. 117 (2019) 299–303.

[4] C. Bouzidi, M. Ferhi, H. Elhouichet, M. Ferid, Structural and luminescence properties of (Ba1−xEux)MoO4 powders, J. Lumin. 179 (2016) 230–235.

[5] R. Chai, Y. Liu, G. Zhang, J. Feng, Q. Kang, In situ preparation and luminescence properties of CaWO4 and CaWO4:Ln (Ln = Eu3+, Tb3+) nanoparticles and transparent CaWO4:Ln/PMMA nanocomposites, J. Lumin. 202 (2018) 65–70.

[6] B. Sun, X.J. Jia, J.H. Wu, P. Chen, Controlled synthesis and room-temperature ferromagnetism of CaWO4 nanostructures, J. Alloy. Comp. 653 (2015) 95–99.

[7] C. Bouzidi, N. Sdiri, A. Boukhachem, H. Elhouichet, M. Férid, Impedance analysis of BaMo1−xWxO4 ceramics, Superlattice Microstruct. 82 (2015) 559–573.

[8] D.W. Kim, I.-S. Cho, S.S. Shin, S. Lee, T.H. Noh, D.H. Kim, H.S. Jung, K.S. Hong, Electronic band structures and photovoltaic properties of MWO4 (M = Zn, Mg, Ca, Sr) compounds, J. Solid State Chem. 184 (2011) 2103–2107.

[9] T. Siritanon, A. Jiamprasertboon, N. Yong, Structure and optical properties of Ni1−xCoxWO4 solid solutions, Mater. Lett. 145 (2015) 316–320.

[10] P.F.S. Pereira, A.F. Gouveia, M. Assis, R.C. de Oliveira, I.M. Pinatti, M. Penha, R.F. Gonçalves, L. Gracia, J. Andrés, E. Longo, ZnWO4 nanocrystals: synthesis, morphology, photoluminescence and photocatalytic properties, Phys. Chem. Chem. Phys. 20 (2018) 1923–1937.

[11] C. Zhang, H. Zhang, K. Zhang, X. Li, Q. Leng, C. Hu, Photocatalytic activity of ZnWO4: band structure, morphology and surface modification, ACS Appl. Mater. Interfaces 6 (2014) 14423–14432.

[12] C. Li, X. Du, D. Yue, J. Gao, Z. Wang, Full-color emission based ZnWO4 spherical nanoparticles through doping of rare earth ions, Mater. Lett. 108 (2013) 257–260.

[13] R.F. Gonçalves, M.J. Godinho, A.P.A. Marques, M.R.C. Santos, I.L.V. Rosa, E. Longo, M.S. Li, J.L.S. Sa, L.S. Cavalcante, Structure, morphology, and optical properties of (Ca1−3xEu2x)WO4 microcrystals, Electr. Mater. Lett. 11 (2015) 193–197.

[14] Y. Yang, X. Wang, B. Liu, Synthesis of cawo4 and cawo4:eu microspheres by precipitation, Nano 09 (2013) 1450008.

[15] G. Chen, F. Wang, W. Ji, Y. Liu, X. Zhang, Improved luminescence of CaWO4:Eu3+

[16] M. Mai, C. Feldmann, Microemulsion-based synthesis and luminescence of nanoparticulate CaWO4, ZnWO4, CaWO4:Tb, and CaWO4:Eu, J. Mater. Sci. 47 (2012) 1427–1435.

[17] Y. Tian, B. Chen, H. Yu, R. Hua, X. Li, J. Sun, L. Cheng, H. Zhong, J. Zhang, Y. Zheng, T. Yu, L. Huang, Controllable synthesis and luminescent properties of three-dimensional nanostructured CaWO4:Tb3+ microspheres, J. Colloid Interface Sci. 360 (2011) 586–592.

[18] J. Han, L. Li, M. Peng, B. Huang, F. Pan, F. Kang, L. Li, J. Wang, B. Lei, Toward Bi3+ red luminescence with No visible reabsorption through manageable energy interaction and crystal defect modulation in single Bi3+-doped ZnWO4 crystal, Chem. Mater. 29 (2017) 8412–8424.

[19] R.S. Yadav, S.J. Dhoble, S.B. Rai, Enhanced photoluminescence in Tm3+, Yb3+, Mg2+ tri-doped ZnWO4 phosphor: three photon upconversion, laser induced optical heating and temperature sensing, Sens. Actuators B Chem. 273 (2018) 1425–1434.

[20] L. Li, F. Qin, Y. Zhou, Y. Zheng, H. Zhao, Z. Zhang, Using the upconversion luminescence of the CaWO4:Yb3+−X3+ (X = Er/Ho/Tm) phosphors for ratiometric thermal sensing, J. Lumin. 202 (2018) 301–308.

[21] Y. Huang, Y. Gao, Q. Zhang, J.-j. Cao, R.-j. Huang, W. Ho, S.C. Lee, Hierarchical porous ZnWO4 microspheres synthesized by ultrasonic spray pyrolysis: characterization, mechanistic and photocatalytic NOx removal studies, Appl. Catal. Gen. 515 (2016) 170–178.

[22] J.L. Rico, M. Albiter, J. Espino, J.S.J. Hargreaves, M. Ostroumov, L.I. Salcedo, K. Wilson, Synthesis and ammonolysis of nickel and cobalt tungstates and their characterisation, J. Saudi Chem. Soc. 20 (2016) 405–410.

[23] X.A. López, A.F. Fuentes, M.M. Zaragoza, J.A. Díaz Guillén, J.S. Gutiérrez, A.L. Ortiz, V. Collins-Martínez, Synthesis, characterization and photocatalytic evaluation of MWO4 (M = Ni, Co, Cu and Mn) tungstates, Int. J. Hydrogen Energy 41 (2016) 23312–23317.

[24] U.M. García-Pérez, A. Martínez-de la Cruz, J. Peral, Transition metal tungstates synthesized by co-precipitation method: basic photocatalytic properties, Electrochim. Acta 81 (2012) 227–232.

[25] X. Zhao, J. Yan, J. Xue, Z. Han, S. Cui, L. Zong, D. Zheng, C. Shen, H. Yu, X. Zhai, Transition-metal ion modified monolacunary tungstates: synthesis, structural characterization and property, Inorg. Chim. Acta 414 (2014) 46–52.

[26] P. Parhi, T.N. Karthik, V. Manivannan, Synthesis and characterization of metal tungstates by novel solid-state metathetic approach, J. Alloy. Comp. 465 (2008) 380–386.

[27] T. Montini, V. Gombac, A. Hameed, L. Felisari, G. Adami, P. Fornasiero, Synthesis, characterization and photocatalytic performance of transition metal tungstates, Chem. Phys. Lett. 498 (2010) 113–119.

[28] A.A.G. Santiago, L.X. Lovisa, P.N. Medeiros, M.S. Li, N.L.V. Carreño, E. Longo, C.A. Paskocimas, M.R.D. Bomio, F.V. Motta, Fast and simultaneous doping of Sr0.9−x−y−zCa0.1In2O4:(xEu3+, yTm3+, zTb3+) superstructure by ultrasonic spray pyrolysis, Ultrason. Sonochem. 56 (2019) 14–24.

[29] A.A.G. Santiago, N.F. Andrade Neto, E. Longo, C.A. Paskocimas, F.V. Motta, M.R.D. Bomio, Fast and continuous obtaining of Eu3+ doped CeO2 microspheres by ultrasonic spray pyrolysis: characterization and photocatalytic activity, J. Mater. Sci. Mater. Electron. 30 (2019) 11508–11519.

[30] H. Choi, S.P. Yoon, J. Han, J. Kim, M.R. Othman, Continuous synthesis of molybdenum oxide microspheres by ultrasonic spray pyrolysis, J. Ind. Eng. Chem. 47 (2017) 254–259.

[31] Z. Cheng, P. Foroughi, A. Behrens, Synthesis of nanocrystalline TaC powders via single-step high temperature spray pyrolysis from solution precursors, Ceram. Int. 43 (2017) 3431–3434.

[32] P.S. Patil, Versatility of chemical spray pyrolysis technique, Mater. Chem. Phys. 59 (1999) 185–198.

[33] A.A.G. Santiago, C.R.R. Almeida, R.L. Tranquilin, R.M. Nascimento, C.A. Paskocimas, E. Longo, F.V. Motta, M.R.D. Bomio, Photoluminescent properties of the Ba1−xZnxMoO4 heterostructure obtained by ultrasonic spray pyrolysis, Ceram. Int. 44 (2018) 3775–3786.

[34] C.R.R. Almeida, L.X. Lovisa, A.A.G. Santiago, M.S. Li, E. Longo, C.A. Paskocimas, F.V. Motta, M.R.D. Bomio, One-step synthesis of CaMoO4: Eu3+ nanospheres by ultrasonic spray pyrolysis, J. Mater. Sci. Mater. Electron. 28 (2017) 16867–16879.

[35] P.N. Medeiros, A.A.G. Santiago, E.A.C. Ferreira, M.S. Li, E. Longo, M.R.D. Bomio, F.V. Motta, Influence Ca-doped SrIn2O4 powders on photoluminescence property prepared one step by ultrasonic spray pyrolysis, J. Alloy. Comp. 747 (2018) 1078–1087.

[36] B. Toby, EXPGUI, a graphical user interface for GSAS, J. Appl. Crystallogr. 34 (2001) 210–213.

[37] H. Rietveld, A profile refinement method for nuclear and magnetic structures, J. Appl. Crystallogr. 2 (1969) 65–71.

[38] P.F. Schofield, K.S. Knight, S.A.T. Redfern, G. Cressey, Distortion characteristics across the structural phase transition in (Cu1-xZnx)WO4, Acta Crystallogr. B 53 (1997) 102–112.

[39] P.F. Schofield, K.S. Knight, G. Cressey, Neutron powder diffraction study of the scintillator material ZnWO4, J. Mater. Sci. 31 (1996) 2873–2877.

[40] R. Burbank, Absolute integrated intensity measurement: application to CaWO4 and comparison of several refinements, Acta Crystallogr. 18 (1965) 88–97.

[41] R.M. Hazen, L.W. Finger, J.W.E. Mariathasan, High-pressure crystal chemistry of scheelite-type tungstates and molybdates, J. Phys. Chem. Solids 46 (1985) 253–263.

[42] G.L. Messing, S.-C. Zhang, G.V. Jayanthi, Ceramic powder synthesis by spray pyrolysis, J. Am. Ceram. Soc. 76 (1993) 2707–2726.

[43] W.M. Haynes, CRC Handbook of Chemistry and Physics, 97 ed., CRC Press, 2016.

[44] L. Tolvaj, K. Mitsui, D. Varga, Validity limits of Kubelka–Munk theory for DRIFT

spectra of photodegraded solid wood, Wood Sci. Technol. 45 (2011) 135–146.

[45] D.L. Wood, J. Tauc, Weak absorption tails in amorphous semiconductors, Phys. Rev. B 5 (1972) 3144–3151.

[46] W. Yan, X. Liu, S. Hou, X. Wang, Study on micro-nanocrystalline structure control and performance of ZnWO4 photocatalysts, Catal. Sci. Technol. 9 (2019) 1141–1153.

[47] A.K. Kunti, N. Patra, S.K. Sharma, H.C. Swart, Radiative transition probability enhancement of white light emitting Dy3+ doped and K+ co-doped BaWO4 phosphors via charge compensation, J. Alloy. Comp. 735 (2018) 2410–2422.

[48] M. Rahmani, T. Sedaghat, A facile sol–gel process for synthesis of ZnWO4 nanopartices with enhanced band gap and study of its photocatalytic activity for degradation of methylene blue, J. Inorg. Organomet. Polym. Mater. 29 (2019) 220–228.

[49] M.M.S. Silva, M.S. Sena, A.L. Lopes-Moriyama, C.P. Souza, A.G. Santos, Experimental planning of the synthesis of strontium molybdate by EDTA-citrate and its structural influence, morphology and optical bandgap, Ceram. Int. 44 (2018) 16606–16614.

[50] G.-T. Xiong, W. Zhang, Z.-F. Hu, P.-J. Hu, Y.-M. Pan, Z.-Y. Feng, L. Ma, Y.-H. Wang, L. Luo, Photocatalytic activity of ZnWO4 phosphors doped with Li impurities, J. Lumin. 206 (2019) 370–375.

[51] Y.A. Sethi, C.S. Praveen, R.P. Panmand, A. Ambalkar, A.K. Kulkarni, S.W. Gosavi, M.V. Kulkarni, B.B. Kale, Perforated N-doped monoclinic ZnWO4 nanorods for efficient photocatalytic hydrogen generation and RhB degradation under natural sunlight, Catal. Sci. Technol. 8 (2018) 2909–2919.

[52] K. Manjunath, C.G. Thimmanna, Effect of organic fuels on surface area and photocatalytic activity of scheelite CaWO4 nanoparticles, Mater. Res. Express 5 (2018) 035030.

[53] A. Sahmi, K. Bensadok, M. Trari, Photoelectrochemical properties of CaWO4 synthetized by chemical route. Application to the phenobarbital electro-photocatalysis, J. Photochem. Photobiol. A Chem. 349 (2017) 36–41.

[54] A. Benmakhlouf, D. Errandonea, A. Bouhemadou, A. Bentabet, S. Maabed, M. Bouchenafa, S. Bin-Omran, Ab initio study of the mechanical and electronic properties of scheelite-type XWO4(X = Ca, Sr, Ba) compounds, Int. J. Mod. Phys. B 31 (2017) 1750086.

[55] M.C. Oliveira, L. Gracia, I.C. Nogueira, M.F.d. Carmo Gurgel, J.M.R. Mercury, E. Longo, J. Andrés, Synthesis and morphological transformation of BaWO4 crystals: experimental and theoretical insights, Ceram. Int. 42 (2016) 10913–10921.

[56] L.S. Cavalcante, V.M. Longo, J.C. Sczancoski, M.A.P. Almeida, A.A. Batista, J.A. Varela, M.O. Orlandi, E. Longo, M.S. Li, Electronic structure, growth mechanism and photoluminescence of CaWO4 crystals, CrystEngComm 14 (2012) 853–868.

[57] R. Lacomba-Perales, J. Ruiz-Fuertes, D. Errandonea, D. Martínez-García, A. Segura, Optical absorption of divalent metal tungstates: correlation between the band-gap energy and the cation ionic radius, EPL (Europhys. Lett.) 83 (2008) 37002.

[58] V.M. Longo, L.S. Cavalcante, A.T. de Figueiredo, L.P.S. Santos, E. Longo, J.A. Varela, J.R. Sambrano, C.A. Paskocimas, F.S. De Vicente, A.C. Hernandes, Highly intense violet-blue light emission at room temperature in structurally disordered SrZrO3 powders, Appl. Phys. Lett. 90 (2007) 091906.

[59] M.A.P. Almeida, J.R.O. Lima, C. Morila-Santos, P.N. Lisboa Filho, M. Siu Li, E. Longo, L.S. Cavalcante, Effect of Zn2+ ions on the structure, morphology and optical properties of CaWO4 microcrystals, J. Sol. Gel Sci. Technol. 72 (2014) 648–654.

[60] Z. Amouzegar, R. Naghizadeh, H.R. Rezaie, M. Ghahari, M. Aminzare, Microwave engineering of ZnWO4 nanostructures: towards morphologically favorable structures for photocatalytic activity, Ceram. Int. 41 (2015) 8352–8359.

[61] Y. Wang, W. Wu, X. Fu, M. Liu, J. Cao, C. Shao, S. Chen, Metastable scheelite CdWO4:Eu3+ nanophosphors: solvothermal synthesis, phase transitions and their polymorph-dependent luminescence properties, Dyes Pigments 147 (2017) 283–290.

[62] G. He, H. Fan, L. Ma, K. Wang, D. Ding, C. Liu, Z. Wang, Synthesis, characterization and optical properties of nanostructured ZnWO4, Mater. Sci. Semicond. Process. 41 (2016) 404–410.

[63] M.F.C. Abreu, F.V. Motta, R.C. Lima, M.S. Li, E. Longo, A.P.d.A. Marques, Effect of process parameters on photophysical properties and barium molybdate phosphors characteristics, Ceram. Int. 40 (2014) 6719–6729.

[64] V.M. Longo, A.T.d. Figueiredo, A.B. Campos, J.W.M. Espinosa, A.C. Hernandes, C.A. Taft, J.R. Sambrano, J.A. Varela, E. Longo, Different origins of green-light photoluminescence emission in structurally ordered and disordered powders of calcium molybdate, J. Phys. Chem. A 112 (2008) 8920–8928.

[65] Y. Zhai, M. Wang, Q. Zhao, J. Yu, X. Li, Fabrication and Luminescent properties of ZnWO4:Eu3+, Dy3+ white light-emitting phosphors, J. Lumin. 172 (2016) 161–167.

[66] T. Yaba, R. Wangkhem, N. Shanta Singh, Photoluminescence properties of Dy3+ activated CaWO4 nanophosphors: a potential single phase near white light emitter, J. Fluoresc. 29 (2019) 435–443.

[67] H.P. Barbosa, I.G.N. Silva, M.C.F.C. Felinto, E.E.S. Teotonio, O.L. Malta, H.F. Brito, Photoluminescence of single-phased white light emission materials based on simultaneous Tb3+, Eu3+ and Dy3+ doping in CaWO4 matrix, J. Alloy. Comp. 696 (2017) 820–827.

[68] S. Das, P. Reed McDonagh, T. Selvan Sakthivel, S. Barkam, K. Killion, J. Ortiz, S. Saraf, A. Kumar, A. Gupta, J. Zweit, S. Seal, Tissue deposition and toxicological effects of commercially significant rare earth oxide nanomaterials: material and physical properties, Environ. Toxicol. 32 (2017) 904–917.

[69] K.T. Rim, K.H. Koo, J.S. Park, Toxicological evaluations of rare earths and their health impacts to workers: a literature review, Saf. Health Work 4 (2013) 12–26.